1 Introduction

There has been much recent theoretical and experimental interest in light dynamics in twisted multi-core optical fibers. Geometries that have been studied include helical waveguides arranged in Lieb lattices [10] and honeycomb lattices [1, 9]. Applications of twisted multi-core fibers include sensors for shape, strain, and temperature [3, 14]. Early work on twisted fibers can be found in [7, 6], in which the coupled mode equations describing light propagation in a circular array of helical waveguides is derived. The introduction of a fiber twist in a circular array allows for control of diffraction and light transfer, in a similar manner to axis bending in linear waveguide arrays [5]. The fiber twist introduces additional phase terms to the model, which is known as the Peierls phase [7, 13]. This system is considered as an optical analogue of topological Aharonov-Bohm suppression in [11]. Parity-time ($\mathcal{PT}$) symmetry in model with balanced gain and loss terms is considered in [8, 2]. In this paper, we consider a multi-core fiber consisting of N waveguides arranged in a ring (Figure 1).

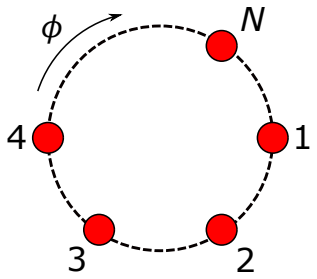

Figure 1: Schematic of N twisted fibers arranged in a ring.

Each fiber is twisted in a uniform fashion along the propagation direction z. For the system with an optical Kerr nonlinearity, the dynamics are given by the coupled system of equations [2, 12]

$$i\partial_z c_n = k\left(e^{-i\phi}c_{n+1} + e^{i\phi}c_{n-1}\right) + i\gamma_n c_n + d|c_n|^2 c_n \tag{1}$$

for $n = 1, \ldots, N$, where $c_0 = c_N$ and $c_{N+1} = c_1$ due to the circular geometry. The quantities $c_n(z)$ are the complex-valued amplitudes of each waveguide, k is the strength of the nearest-neighbor coupling, γ_n is the optical gain or loss at site n, and ϕ is a parameter representing the twist of the fibers. (See [2, section 2] for a description of the parameters in terms of the optical waveguide system). If $\gamma_n = 0$ for all n, i.e. there is no gain or loss at each node, equation (1) becomes

$$i\partial_z c_n = k\left(e^{-i\phi}c_{n+1} + e^{i\phi}c_{n-1}\right) + i\gamma_n c_n + d|c_n|^2 c_n, \tag{2}$$

which is Hamiltonian with energy given by

$$H = \sum_{n=1}^{N} k(c_{n+1}c_n^* e^{-i\phi} + c_n c_{n+1}^* e^{i\phi}) + \frac{d}{2}|c_n|^4. \tag{3}$$

The system with no gain or loss is considered in [2]. Asymptotic analysis for the case of $N = 6$ fibers where the peak intensity is contained in the first fiber ($n = 1$) is used to demonstrate that the opposite fiber in the ring ($n = 4$) has, to leading order, zero intensity when the twist parameter is given by $\phi = \pi/6$. This is confirmed by numerical time evolution simulations (see [2, Figures 4 and 5]). This phenomenon is discussed in the context of Aharonov-Bohm-like suppression of optical tunneling in twisted multicore fibers in [12]; in particular, this effect is demonstrated analytically for the case of $N = 4$ fibers by solving the nonlinear system (1) analytically.

In this paper, we study standing wave solutions (bound states) of equation (1). This paper is organized as follows. In section 2, we construct standing wave solutions to (1).

2 Standing wave solutions

Standing wave solutions to (2) are bound states of the form

$$c_n = a_n e^{i(\omega z + \theta_n)}, \tag{4}$$

where $a_n \in \mathbb{R}$, $\theta_n \in (-\pi/2, \pi/2]$, and ω is the frequency of oscillation. (Since a_n can be negative, we can restrict θ_n to that interval). Making this substitution and simplifying, equation (2) becomes

$$k\left(a_{n+1}e^{i((\theta_{n+1}-\theta_n)-\phi)} + a_{n-1}e^{-i((\theta_n-\theta_{n-1})-\phi)}\right) + \omega a_n + d a_n^3 = 0, \tag{5}$$

which can be written as the system of $2n$ equations

$$\begin{aligned} &k\left(a_{n+1}\cos(\theta_{n+1}-\theta_n-\phi) + a_{n-1}\cos(\theta_n-\theta_{n-1}-\phi)\right) + \omega a_n + d a_n^3 = 0 \\ &a_{n+1}\sin(\theta_{n+1}-\theta_n-\phi) - a_{n-1}\sin(\theta_n-\theta_{n-1}-\phi) = 0 \end{aligned} \tag{6}$$

by separating real and imaginary parts. We note that the the exponential terms in (5) depend only on the phase differences $\theta_{n+1} - \theta_n$ between adjacent sites. Due to the gauge invariance of (2), if c_n is solution, so is $e^{i\theta}c_n$, thus we may without loss of generality take $\theta_1 = 0$. If $\phi = 0$, i.e. the fibers are not twisted, we can take $\theta_n = 0$ for all n, and so (5) reduces to the untwisted case with periodic boundary conditions. Similarly, if we take $\phi = 2\pi/N$ and $\theta_n = (n-1)\phi$ for all n, the exponential terms do not contribute, and (5) once again reduces to untwisted case. The interesting case, therefore, occurs when $0 < \theta < 2\pi/N$.

In the anti-continuum (AC) limit, which occurs when $k = 0$, the sites are decoupled. Each a_n can take on the values $\{0, \pm\sqrt{-\omega/d}\}$, the phases θ_n are arbitrary, and ϕ does not contribute. The amplitudes $\sqrt{-\omega/d}$ are real if d and ω have opposite signs. We construct solutions to (6) by parameter continuation from the AC limit with no twist using AUTO. As an initial condition, we choose a single excited site at node 1, i.e. $a_1 = \sqrt{-\omega/d}$ and $a_n = 0$ for all other n; for the phases, $\theta_n = 0$ for all n, and we also take $\phi = 0$. (We can start with more than once excited state, but, in general, these solutions will not be stable.) We first continue in the coupling parameter k, and then, for fixed k, we continue in the twist parameter ϕ. In doing this, we observe that the solutions have the following symmetry:

$$\begin{aligned} a_k &= a_{N-k+2} \qquad && k = 2, \ldots, M-1 \\ \theta_k &= -a_{N-k+2} \qquad && k = 2, \ldots, M-1, \end{aligned} \tag{7}$$

where $M = (N/2) + 1$ for N even and $M = (N+1)/2$ for N odd. For N even, node M is the node directly across the ring from node 1, and $\theta_M = 0$. For all N, $\theta_1 = 0$. See Figure 2 for an illustration of these symmetry relations for $N = 6$ and $N = 7$.

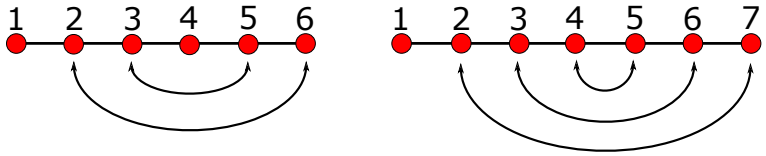

Figure 2: Schematic of symmetry relationship between nodes for $N = 6$ and $N = 7$. For nodes connected with arrows, the amplitudes a_k are the same and the phases θ_k are opposite.

Figure 3 shows an example of a standing wave solution produced by numerical parameter continuation for $N = 6$. The symmetry relations (7) among the amplitudes a_k can be seen in the right panel.

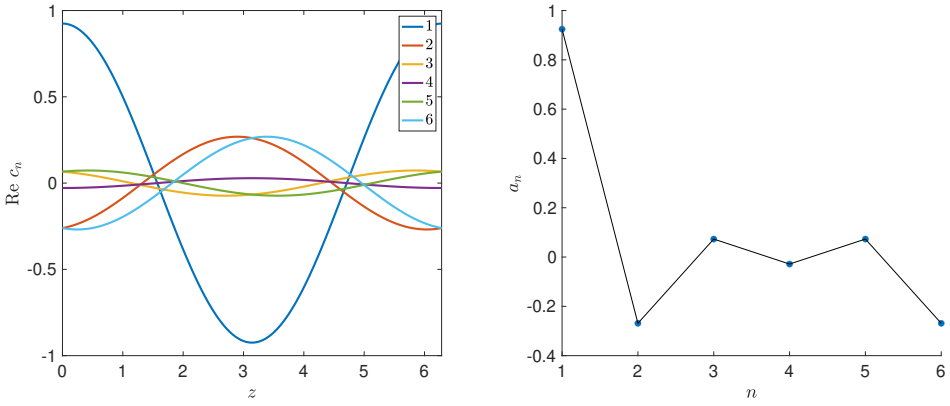

Figure 3: Standing wave solution for $N = 6$, $\omega = 1$, and $\phi = 0.25$. Left is real part of solution c_n versus z for each node over a full period (2π), right is amplitude a_n solution at each node. $k = 0.25$, $d = -1$.

2.1 N even

Numerical parameter continuation for N even, starting from a single excited node at node 1, suggests that when the twist parameter $\phi = \pi/N$, the opposite node is completely dark, i.e. has an amplitude of 0. Using the symmetries (7), when $a_M = 0$, the system (6) reduces

to

$$\begin{aligned}
&2ka_2\cos(\theta_2-\phi)+\omega a_1+da_1^3=0\\
&k(a_{n+1}\cos(\theta_{n+1}-\theta_n-\phi)+a_{n-1}\cos(\theta_n-\theta_{n-1}-\phi))+\omega a_n+da_n^3=0 \quad n=2,\dots,M-1\\
&a_{n+1}\sin(\theta_{n+1}-\theta_n-\phi)-a_{n-1}\sin(\theta_n-\theta_{n-1}-\phi)=0 \qquad\qquad n=2,\dots,M-1\\
&2ka_{M-1}\cos(\theta_{M-1}+\phi)=0\\
&\theta_1=\theta_M=0.
\end{aligned} \tag{8}$$

It follows that $a_n = 0$ for all n unless

$$\begin{aligned}
&\cos(\theta_{M-1}+\phi)=0\\
&\sin(\theta_n-\theta_{n-1}-\phi)=0 \qquad n=3,\dots,M-1\\
&\sin(\theta_2-\phi)=0.
\end{aligned} \tag{9}$$

One solution to this is

$$\begin{aligned}
&\theta_{M-1}+\phi=\pi/2\\
&\theta_n-\theta_{n-1}-\phi=0 \quad n=3,\dots,M-1\\
&\theta_2-\phi=0,
\end{aligned} \tag{10}$$

from which it follows that we can have a single dark node at site M when $\phi = \pi/N$. If this is the case, the system of equations (8) reduces to the simpler system

$$\begin{aligned}
&2ka_2+\omega a_1+da_1^3=0\\
&k\left(a_{n+1}+a_{n-1}\right)+\omega a_n+da_n^3=0 \qquad n=2,\dots,M-2\\
&ka_{M-2}+\omega a_{M-1}+da_{M-1}^3=0.
\end{aligned} \tag{11}$$

This system is of the form $F(a,k) = 0$, where $a = (a_1,\dots,a_{M-1})$. $F(\tilde{a},0) = 0$, where $\tilde{a} = (\sqrt{-\omega/d},0,\dots,0)$. Since $D_F(\tilde{a},0) = \mathrm{diag}(-2\omega,\omega,\dots,\omega)$, which is invertible for $\omega \neq 0$, the system (11) has a solution for sufficiently small k by the implicit function theorem. Once (11) has been solved, we obtain the full solution to (6) using

$$\begin{aligned}
&a_M=0\\
&a_{M+k}=a_{M-k} && k=1,\dots,M-2\\
&\theta_0=0\\
&\theta_k=(k-1)\phi && k=2,\dots,M-1\\
&\theta_M=0\\
&\theta_{M+k}=-\theta_{M-k} && k=1,\dots,M-2.
\end{aligned}$$

Figure 4 shows this solution for $N = 6$. This observation of a dark node for $N = 6$ when $\phi = \pi/6$ agrees with what was shown in [2].

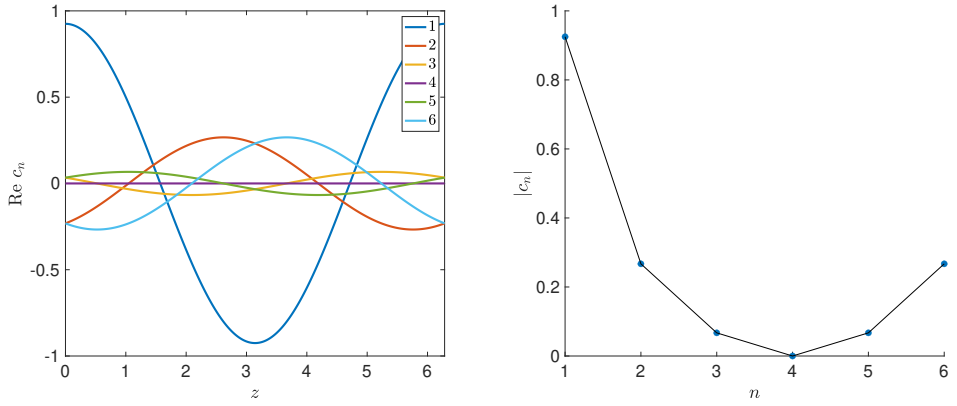

Figure 4: Standing wave solution for $N = 6$ and $\phi = \pi/6$. Left is real part of solution for each node, right is absolute value of solution at each node. Node 1 has maximum amplitude, and node 4 is a dark node. $\omega = 1$, $k = 0.25$, $d = -1$.

Numerical parameter continuation with AUTO shows that these standing wave solutions exist for $|k| \leq k_0$, where k_0 depends on N and ω but not d (Figure 5, left panel). The dependence of k_0 on ω is shown in the right panel of Figure 5, which suggests that k_0 approaches $\omega/2$ as N gets large. As the parameter continuation approaches k_0, the solution approaches the zero solution.

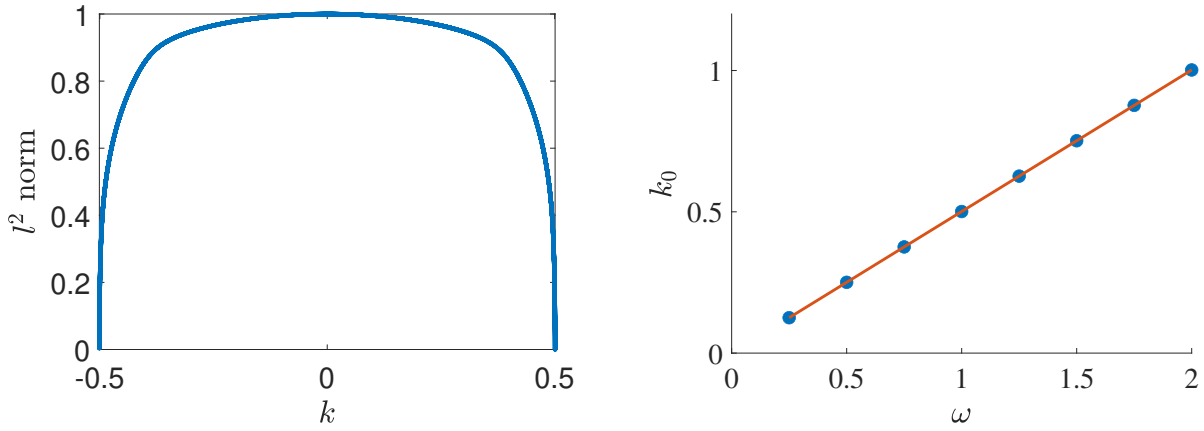

Figure 5: Left panel shows l^2 norm of solution vs k, for $N = 50$ with dark node at node 4, $\omega = 1$, and $d = -1$. Right panel shows k_0 vs ω together with least squares linear regression line for $N = 50$ and $d = -1$.

2.2 N odd

We can also obtain a dark node when N is odd by taking node 1 to be the dark node; in this case, the dark node will be opposite a pair of bright nodes at a_M and a_{M+1} with the same

amplitude. Using the symmetries (7), when $a_1 = 0$, the system (6) reduces to

$$\begin{aligned}
&2ka_2\cos(\theta_2-\phi)=0\\
&ka_3\cos(\theta_3-\theta_2-\phi)+\omega a_2+da_2^3=0\\
&a_3\sin(\theta_3-\theta_2-\phi)=0\\
&k\left(a_{n+1}\cos(\theta_{n+1}-\theta_n-\phi)+a_{n-1}\cos(\theta_n-\theta_{n-1}-\phi)\right)+\omega a_n+da_n^3=0 \quad n=3,\dots,M-1\\
&a_{n+1}\sin(\theta_{n+1}-\theta_n-\phi)-a_{n-1}\sin(\theta_n-\theta_{n-1}-\phi)=0 \qquad\qquad n=3,\dots,M-1\\
&k(a_M\cos(-2\theta_M-\phi)+a_{M-1}\cos(\theta_M-\theta_{M-1}-\phi))+\omega a_M+da_M^3=0\\
&a_M\sin(-2\theta_M-\phi)-a_{M-1}\sin(\theta_M-\theta_{M-1}-\phi)=0.
\end{aligned} \tag{12}$$

It follows that $a_n = 0$ for all n unless

$$\begin{aligned}
&\cos(\theta_2-\phi)=0\\
&\sin(\theta_n-\theta_{n-1}-\phi)=0 \qquad n=3,\dots,M-1\\
&\sin(2\theta_M+\phi)=0.
\end{aligned} \tag{13}$$

One solution to this is

$$\begin{aligned}
&\theta_2-\phi=-\pi/2\\
&\theta_n-\theta_{n-1}-\phi=0 \qquad n=3,\dots,M-1\\
&2\theta_M+\phi=0,
\end{aligned} \tag{14}$$

from which it follows that we can have a single dark node at a_1 when $\phi = \pi/N$. This condition for a dark node is the same as for the N even case. For this case, (12) reduces to the simpler system of equations

$$\begin{aligned}
&ka_3+\omega a_2+da_2^3=0\\
&k(a_{n+1}+a_{n-1})+\omega a_n+da_n^3=0 \qquad n=3,\dots,M-1\\
&k(a_M+a_{M-1})+\omega a_M+da_M^3=0.
\end{aligned} \tag{15}$$

This system of equations is again of the form $F(a,k)=0$, where $a=(a_2,\dots,a_M)$. $F(\tilde{a},0)=0$, where $\tilde{a}=(0,\dots,0,\sqrt{-\omega/d},0)$. Since $D_F(\tilde{a},0)=\mathrm{diag}(\omega,\dots,\omega,-2\omega)$, which is invertible for $\omega\neq 0$, the system (15) has a solution for sufficiently small k by the implicit function theorem. Once (15) has been solved, we obtain the full solution to (6) using

$$\begin{aligned}
&a_1=0\\
&a_{M+k}=a_{M-k+1} && k=1,\dots,M-1\\
&\theta_0=0\\
&\theta_k=(k-1)\phi-\pi/2 && k=2,\dots,M\\
&\theta_{M+k}=-\theta_{M-k+1} && k=1,\dots,M-1
\end{aligned}$$

Figure 6 shows this solution for $N = 7$. The results of parameter continuation experiments are similar to that of the N even case.

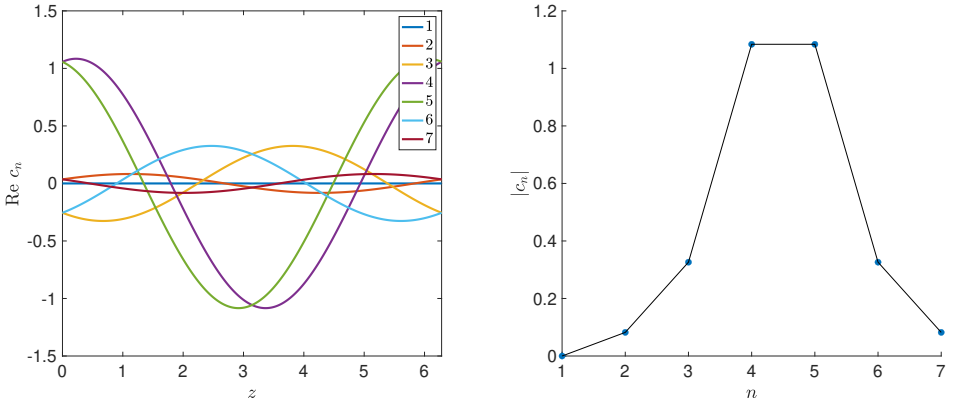

Figure 6: Standing wave solution for $N = 7$ and $\phi = \pi/7$. Left is real part of solution for each node, right is absolute value of solution at each node. Nodes 4 and 5 have equal and maximum amplitude, and node 1 is a dark node. $\omega = 1$, $k = 0.25$, $d = -1$.

3 Stability

We now look at the stability of the standing wave solutions we constructed in the previous section. The linearization of (2) about a standing wave solution $c_n = a_n e^{i(\omega z + \theta_n)} = (v_n + iw_n)e^{i\omega z}$ is the $2N \times 2N$ block matrix

$$A(c_n) = k \begin{pmatrix} S & C \\ -C & S \end{pmatrix} + \omega \begin{pmatrix} 0 & I \\ -I & 0 \end{pmatrix} \tag{16}$$

$$- \begin{pmatrix} \operatorname{diag}(2v_n w_n) & \operatorname{diag}(v_n^2 + 3w_n^2) \\ -\operatorname{diag}(3v_n^2 + w_n^2) & -\operatorname{diag}(2v_n w_n) \end{pmatrix} \tag{17}$$

where each block is $N \times N$, C is the periodic banded matrix with $\cos\phi$ on the first upper and lower diagonals, and S is the periodic banded matrix with $\sin\phi$ on the first lower diagonal and $-\sin\phi$ on the first upper diagonal:

$$C = \begin{pmatrix} 0 & \cos\phi & & \dots & \cos\phi \\ \cos\phi & 0 & \cos\phi & & \\ & \ddots & \ddots & & \\ \cos\phi & & \dots & \cos\phi & 0 \end{pmatrix}$$

$$S = \begin{pmatrix} 0 & -\sin\phi & & \dots & \sin\phi \\ \sin\phi & 0 & -\sin\phi & & \\ & \ddots & \ddots & & \\ -\sin\phi & & \dots & \sin\phi & 0 \end{pmatrix}.$$

Since (16) is a finite dimensional matrix, the spectrum is purely point spectrum. Due to the gauge invariance, there an eigenvalue at 0 with algebraic multiplicity 2 and geometric multiplicity 1. Following the analysis in [4, Section 2.1.1.1], there are plane wave eigenfunctions

which are, to leading order, of the form $e^{\pm(iqn+\lambda z)}$ and satisfy the dispersion relation

$$\lambda = \pm i\left(\omega + 2k\cos(q+\phi)\right). \tag{18}$$

The corresponding eigenvalues are thus purely imaginary and are contained in the bounded intervals $\pm i[\omega - 2k, \omega + 2k]$. As N increases, these eigenvalues fill out this interval. For $|k| < k_0 = \omega/2$, these eigenvalues cannot interact with the kernel eigenvalues. Figure 7 illustrates these results numerically for $\omega = 1$ and $k = 0.25$ for the case of N even with a single dark node opposite a bright node. Similar results are obtained for other values of ω and k and for all other solutions generated from the AC limit starting with a single excited node.

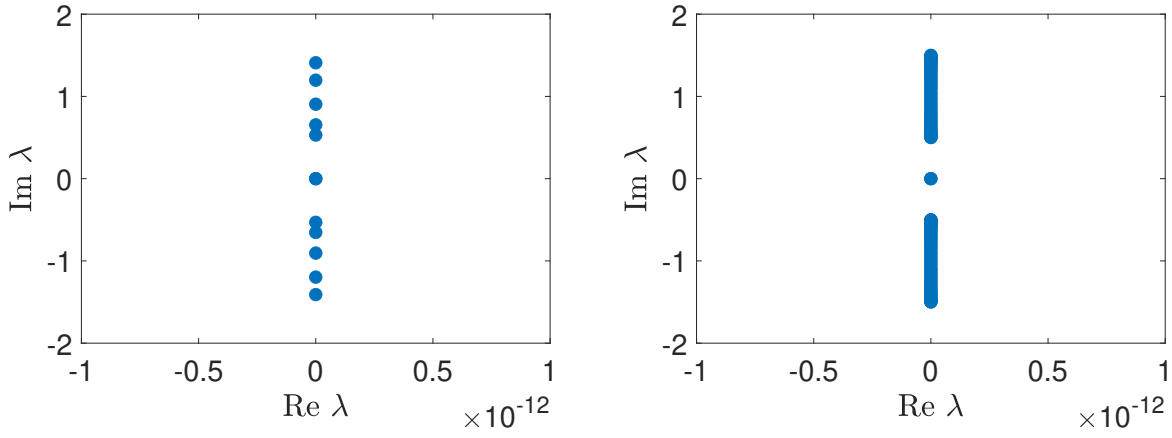

Figure 7: Spectrum of linearization of (2) about solution for even N with a single dark node opposite a single bright node. $N = 6$ (left panel) and $N = 50$ (left panel). $k = 0.25$, $\omega = 1$, $\phi = \pi/N$.

Since the spectrum of these solutions is purely imaginary, we expect that they will be neutrally stable. Figure 8 shows the results of timestepping for a small perturbation of the standing wave solution when $N = 6$. The solutions show small oscillations but no growth, suggesting neutral stability. Similar results are obtained for other values of N for N even, N odd with a dark node opposite a pair of bright nodes, and general N with a single bright node. In addition, if we start with a neutrally stable standing wave solution and perturb the system by a small change in k or ϕ, the time evolution resembles that in Figure 8.

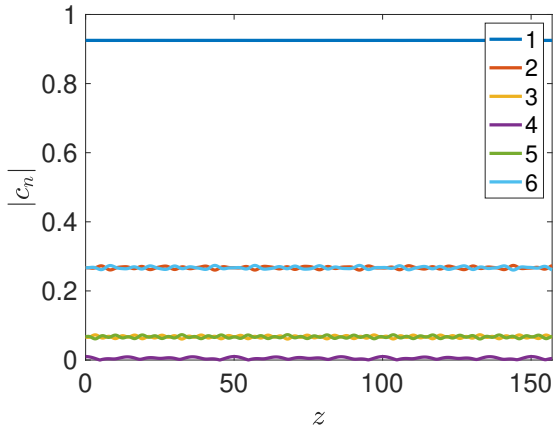

Figure 8: $|c_n|$ versus z for solution with $N = 6$ and a single dark node opposite a bright node. Initial condition is perturbed by adding 0.01 to dark node. Timestepping using a fourth order Runge-Kutta scheme. $k = 0.25$, $d = -1$, $\phi = \pi/6$.

4 Variants

If the strength of the nearest-neighbor coupling is allowed to differ between pairs of nodes, equation (2) becomes

$$i\partial_z c_n = k_{n+1}e^{-i\phi}c_{n+1} + k_{n-1}e^{i\phi}c_{n-1} + i\gamma_n c_n + d|c_n|^2 c_n. \tag{19}$$

This allows for asymmetric solutions, as shown in Figure 9. (Contrast to the symmetric solutions for uniform k in Figure 3). These asymmetric solutions are also neutrally stable.

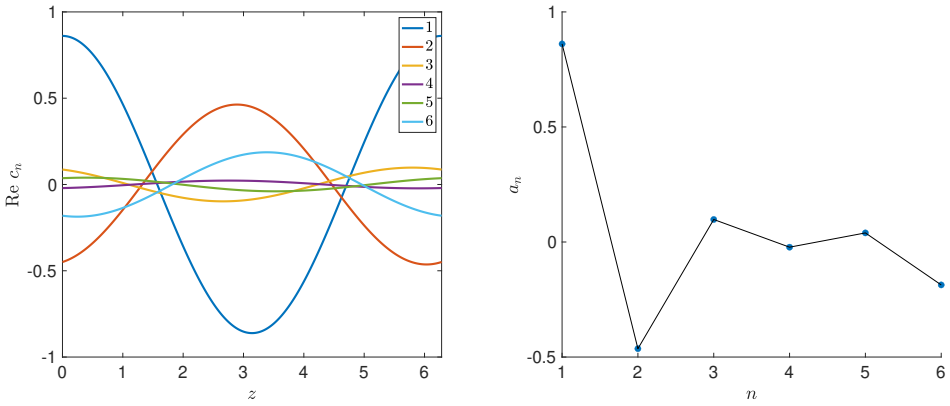

Figure 9: Standing wave solution to (19) for $N = 6$. $\omega = 1$, $k_1 = 0.4$, and $k_n = 0.2$ for all other n. Left is real part of solution c_n versus z for each node over a full period (2π), right is amplitude a_n solution at each node. $\phi = 0.25$, $d = -1$.

5 Conclusions

Acknowledgments This material is based upon work supported by the U.S. National Science Foundation under the RTG grant DMS-1840260 (R.P. and A.A.).

References

[1] Mark J. Ablowitz, Christopher W. Curtis, and Yi-Ping Ma, *Linear and nonlinear traveling edge waves in optical honeycomb lattices*, Phys. Rev. A **90** (2014), 023813.

[2] Yannan; Srinivasan Gowri; Aceves Alejandro B.; Kevrekidis Panayotis G. Castro-Castro, Claudia; Shen, *Light dynamics in nonlinear trimers and twisted multicore fibers*, Journal of Nonlinear Optical Physics and Materials **25** (2016).

[3] P. S.; Feder K. S.; Kremp T.; Taunay T. F.; Monberg E.; Kelliher J.; Ortiz R.; Bradley K.; Abedin K. S.; Au D.; Puc G. Gannot, Israel; Westbrook, *Spie proceedings [spie spie bios - san francisco, california, united states (saturday 1 february 2014)] optical fibers and sensors for medical diagnostics and treatment applications xiv - integrated optical fiber shape sensor modules based on twisted multicore fiber grating arrays*, vol. 8938, 2014.

[4] Panayotis G. Kevrekidis, *The discrete nonlinear Schrödinger equation*, Springer Berlin Heidelberg, 2009.

[5] Stefano Longhi, *Self-imaging and modulational instability in an array of periodically curved waveguides*, Optics Letters **30** (2005).

[6] ———, *Bloch dynamics of light waves in helical optical waveguide arrays*, Physical Review B **76** (2007).

[7] ———, *Light transfer control and diffraction management in circular fibre waveguide arrays*, Journal of Physics B Atomic Molecular and Optical Physics **40** (2007).

[8] Stefano Longhi, *Pt phase control in circular multi-core fibers*, Opt. Lett. **41** (2016), no. 9, 1897–1900.

[9] Yaakov Lumer, Yonatan Plotnik, Mikael C. Rechtsman, and Mordechai Segev, *Self-localized states in photonic topological insulators*, Phys. Rev. Lett. **111** (2013), 243905.

[10] Jeremy L. Marzuola, Mikael Rechtsman, Braxton Osting, and Miguel Bandres, *Bulk soliton dynamics in bosonic topological insulators*, 2019.

[11] G. Della; Gatti D.; Longhi S. Ornigotti, M.; Valle, *Topological suppression of optical tunneling in a twisted annular fiber*, Physical Review A **76** (2007).

[12] Midya Parto, Helena Lopez-Aviles, Mercedeh Khajavikhan, Rodrigo Amezcua-Correa, and Demetrios N. Christodoulides, *Topological aharonov-bohm suppression of optical tunneling in twisted nonlinear multicore fibers*, Phys. Rev. A **96** (2017), 043816.

[13] R. Peierls, *Zur Theorie des Diamagnetismus von Leitungselektronen*, Zeitschrift für Physik **80** (1933), no. 11-12, 763–791.

[14] Paul Westbrook, K.S. Feder, Tristan Kremp, W. Ko, Hongchao Wu, E. Monberg, Debra Simoff, and K. Bradley, *Distributed sensing over meter lengths using twisted multicore optical fiber with continuous Bragg gratings*, Furukawa Review (2017), 26–32.